

# Mass Outflow in the Seyfert 1 Galaxy NGC 5548<sup>1</sup>

D.M. Crenshaw<sup>2</sup>, S.B. Kraemer<sup>3</sup>, H.R. Schmitt<sup>4</sup>, J.S. Kaastra<sup>5,6</sup>, N. Arav<sup>7</sup>, J.R. Gabel<sup>8</sup>,  
and K.T. Korista<sup>9</sup>

## ABSTRACT

We present a study of the intrinsic UV absorption and emission lines in an historically low-state spectrum of the Seyfert 1 galaxy NGC 5548, which we obtained in 2004 February at high spatial and spectral resolution with the Space Telescope Imaging Spectrograph (STIS) on the *Hubble Space Telescope (HST)*. We isolate a component of emission with a width of  $680 \text{ km s}^{-1}$  (FWHM) that arises from an “intermediate line region” (ILR), similar to the one we discovered in NGC 4151, at a distance of  $\sim 1$  pc from the central continuum source. From a detailed analysis of the five intrinsic absorption components in NGC 5548 and their behavior over a span of 8 years, we present evidence that most of the UV absorbers only partially cover the ILR and do not cover an extended region of UV continuum emission, most likely from hot stars in the circumnuclear region. We also find that four of the UV absorbers are at much greater distances ( $>70$  pc) than the ILR, and none have sufficient N V or C IV column densities to be the ILR in absorption. At least a portion of the UV absorption component 3,

---

<sup>1</sup>Based on observations made with the NASA/ESA Hubble Space Telescope, obtained at the Space Telescope Science Institute, which is operated by the Association of Universities for Research in Astronomy, Inc., under NASA contract NAS 5-26555. These observations are associated with proposal 9511.

<sup>2</sup>Department of Physics and Astronomy, Georgia State University, Astronomy Offices, One Park Place South SE, Suite 700, Atlanta, GA 30303; crenshaw@chara.gsu.edu

<sup>3</sup>Institute for Astrophysics and Computational Sciences, Department of Physics, The Catholic University of America, Washington, DC 20064

<sup>4</sup>Remote Sensing Division, Naval Research Laboratory, Washington, DC 20375; and Interferometrics, Inc., Herndon, VA 20171

<sup>5</sup>SRON Netherlands Institute for Space Research, Sorbonnelaan 2, 3584 CA Utrecht, The Netherlands

<sup>6</sup>Sterrenkundig Instituut, Universiteit Utrecht, P.O. Box 80000, 3508 TA Utrecht, The Netherlands

<sup>7</sup>Physics Department, Virginia Polytechnic Institute & State University, Blacksburg, VA 24061

<sup>8</sup>Physics Department, Creighton University, Omaha NE 68178

<sup>9</sup>Department of Physics, Western Michigan University, Kalamazoo, MI 49008

at a radial velocity of  $-530 \text{ km s}^{-1}$ , is likely responsible for most of the X-ray absorption, at a distance  $< 7 \text{ pc}$  from the central source. The fact that we see the ILR in absorption in NGC 4151 and not in NGC 5548 suggests that the ILR is located at a relatively large polar angle ( $\sim 45^\circ$ ) with respect to the narrow-line region outflow axis.

*Subject headings:* galaxies: Seyfert – galaxies: individual (NGC 5548)

## 1. Introduction

About 50% of Seyfert 1 galaxies show intrinsic absorption lines in their UV spectra that are blueshifted with respect to their host galaxies (Crenshaw et al. 1999; Dunn et al. 2008), indicating mass outflow from their nuclei. The mass outflow rates are comparable to the accretion rates needed to power the central AGN, indicating the importance of outflows in the overall structure and energetics of active supermassive black holes (SMBHs). Detailed studies of the absorption lines in nearby Seyfert galaxies have shown that many are variable in their ionic column densities over time scales of years, and, in a few cases, weeks to months (cf. Gabel et al. 2005). The variability has been attributed to changes in the ionizing continuum flux incident on the “absorbers”, changes in the total column density in the line of sight (e.g., due to transverse motion of the absorbers against the background emission source), or a combination of the two. In addition, changes in the fraction of the background emission that is covered by the absorber can be interpreted as transverse motion of the absorber (Crenshaw, Kraemer, & Gabel 2004). In general, variability studies provide valuable clues to the physical conditions, geometry, and dynamics of the outflowing absorbers, and, in particular, they provide important information on number densities, distances from the central continuum source (presumed to be the accretion disk and corona around the SMBH), and transverse velocities (Crenshaw, Kraemer, & George 2003).

NGC 5548 ( $z = 0.01676^1$ ) shows multiple kinematic components of  $\text{Ly}\alpha$ , N V, and C IV absorption in high-resolution ( $R = \lambda/\Delta\lambda \geq 10,000$ ) UV spectra (Crenshaw et al. 1999; Mathur et al. 1999), at radial velocities of  $-170$  to  $-1040 \text{ km s}^{-1}$  with respect to

---

<sup>1</sup>We use this heliocentric emission-line redshift to be consistent with our earlier papers. The NASA Extragalactic Database gives the H I 21-cm redshift  $z = 0.017175$  from Springob et al. (2005). If this value is used, the radial velocities of the emission and absorption features in the current paper should be offset by an additional  $-125 \text{ km s}^{-1}$ .

the above redshift. Multiple components of X-ray absorption are also present in grating spectra from the *Chandra X-ray Observatory CXO* (Steenbrugge et al. 2005), although the resolution is not sufficient to identify and resolve all of the velocity components seen in the UV. In our previous papers (Crenshaw & Kraemer 1999, hereafter Paper I; Crenshaw et al. 2003, hereafter Paper II), we probed the physical conditions in the UV absorbers with spectra from the Goddard High-Resolution Spectrograph (GHRS) and Space Telescope Imaging Spectrograph (STIS) onboard the *Hubble Space Telescope (HST)*. We also presented evidence that a couple of the absorbers showed variable ionic column densities.

In this paper, we present new *HST/STIS* observations obtained in 2004 February, when the UV continuum and broad-line region (BLR) fluxes were at an all-time low in the previous 26-year history of satellite UV observations. It appears that NGC 5548 was in a low flux state for several years around this time. Low X-ray fluxes were detected with *CXO* in 2005 April (Detmers et al. 2008), and low BLR and continuum fluxes were observed in the optical during 2005 March – April (Bentz et al. 2007). Long-term monitoring with *RXTE* indicates that X-ray fluxes were in an overall low, but still variable, state during the years 2004 – 2006 (Detmers et al. 2008).

Our recent results on the UV absorption and emission lines in another Seyfert 1 galaxy, NGC 4151 (Crenshaw & Kraemer 2007), illustrate the importance of low-state observations in constraining the properties of mass outflow in AGN. Using STIS echelle observations of NGC 4151, we identified a component of emission with an intermediate width (FWHM =  $1170 \text{ km s}^{-1}$ ) between that of the BLR (FWHM =  $9500 \text{ km s}^{-1}$ ) and the narrow-line region (NLR) (FWHM =  $250 \text{ km s}^{-1}$ ). We were able to isolate this component by choosing a spectrum in a low-flux state, which greatly reduced the BLR contribution to the emission, and by using a small aperture ( $0''.2 \times 0''.2$ ), which significantly reduced the NLR contribution. Based on similar velocity coverages, distances from the continuum source, and physical conditions, we argued that the emission from this “intermediate-line region” (ILR) and the broad, deep absorption in NGC 4151, at a radial velocity of  $-490 \text{ km s}^{-1}$ , arise in the same gas. Linking the ILR emission to the broad absorption provided additional constraints on the mass outflow in NGC 4151, such as the global covering factor ( $\sim 0.4$ ), the outflow rate ( $\sim 0.16 \text{ M}_{\odot} \text{ yr}^{-1}$ ) and the outflow direction (centered on the accretion disk axis at polar angles  $< 55^{\circ}$ ). Additional observations of Seyfert 1 galaxies at low states are important for testing the generality of these results, and we present one such study here for NGC 5548.

## 2. Observations

We obtained STIS echelle spectra of the nucleus of NGC 5548 with the E140M grating through a  $0''.2 \times 0''.2$  aperture. We acquired the observations over five consecutive *HST* orbits on each of four consecutive days in 2004 February, for a total of 20 orbits. In Table 1, we list the details of the new observations as well as the previous *HST* observations at high spectral resolution in the far-UV; the latter are described in more detail in Papers I and II. The two GHRS observations cover the N V and C IV lines separately, and were acquired  $\sim 6$  months apart, when NGC 5548 was at quite different continuum levels (see Paper II). We averaged the spectra from 2004 February, as we had done for 2002 January, because we saw no significant continuum variability ( $\geq 3\%$ ) over these daily intervals. The average 2004 February spectrum has a total exposure time of 52,156 s, which provides sufficient signal-to-noise for a detailed analysis of this very low state. All together, we have five epochs of UV continuum observations and four epochs of high resolution N V and/or C IV observations.

In Figure 1, we show the *HST* high-resolution spectra in the region around C IV. The 2004 spectrum was obtained at a record low continuum flux ( $F_\lambda[1360 \text{ \AA}] = 2.4 (\pm 0.8) \times 10^{-15} \text{ ergs s}^{-1} \text{ cm}^{-2} \text{ \AA}^{-1}$ ) within the 26 years of UV observations (see the light curve in Paper II), which is  $\sim 4.5$  times lower than the previous record set on 1992 July 5 ( $F_\lambda[1360 \text{ \AA}] = 1.07 (\pm 0.17) \times 10^{-14} \text{ ergs s}^{-1} \text{ cm}^{-2} \text{ \AA}^{-1}$ ). The broad C IV emission-line flux, which extends far beyond the range of the plot in Figure 1, is also severely diminished with respect to previous observations. Most of the remaining flux in this region is due to C IV emission from an intermediate-width component, with a full-width at half-maximum (FWHM) of  $\sim 700 \text{ km s}^{-1}$ , compared to the widths of the lines from the BLR and NLR. The five major kinematic components of absorption have maintained their presence throughout the  $\sim 8$  years of high-resolution UV observations<sup>2</sup>, despite a wide range in continuum flux levels. We find no evidence for the appearance of new components or the disappearance of previous components of intrinsic absorption, which we have seen in the Seyfert 1 galaxies NGC 3783 (Kraemer, Crenshaw, & Gabel 2001; Gabel et al. 2005) and NGC 3516 (Kraemer et al. 2002).

## 3. Emission Lines

The intermediate-width emission in the 2004 spectrum resembles that seen in low-state STIS echelle observations of NGC 4151 (Crenshaw & Kraemer 2007). We therefore used the

---

<sup>2</sup>Component 5 is detected as a weak depression in the C IV region in 2004; it is more clearly seen as a distinct feature in N V (see §3).

same approach to quantify this component in NGC 5548. We used He II  $\lambda 1640$  to construct emission-line templates, because it is a non-resonance line and is unaffected by intrinsic absorption. It appears to have two emission components, which we show in Figure 2. We fitted the He II emission-line profile with two Gaussians, after subtracting a continuum spline fit over a much larger wavelength region. The widths of the two Gaussians are  $\text{FWHM} = 260$  and  $680 \text{ km s}^{-1}$ , which we associate with the NLR (in the  $0''.2 \times 0''.2$  aperture, which is  $70 \text{ pc} \times 70 \text{ pc}$  in the plane of the sky at the distance of NGC 5548) and an intermediate-line region (ILR). By comparison, the FWHMs for these components in NGC 4151 are  $250$  and  $1100 \text{ km s}^{-1}$ . As can be seen in Figure 2, the NLR template is slightly redshifted (by  $120 \text{ km s}^{-1}$ ) with respect to the ILR template. The BLR contribution to He II, which lies on the red wing of C IV, is undetectable. Our effectiveness in isolating the ILR component in these two Seyferts can be attributed to the reduction of the NLR contribution by the small aperture and the reduction of the BLR contribution due to the low flux state.

To model the emission-line profiles of the other strong lines, we used the Gaussian profiles from the He II fit as templates. We reproduced the templates at the expected positions of the other strong lines (Ly $\alpha$   $\lambda 1215.670$ ; N V  $\lambda\lambda 1238.821, 1242.804$ ; and C IV  $\lambda\lambda 1548.202, 1550.774$ ), retaining the same velocity widths and preserving the  $-120 \text{ km s}^{-1}$  offset between the NLR and ILR components, and scaled them in intensity until we obtained suitable matches. We allowed the doublet line ratios (e.g., C IV  $\lambda 1548.202/\lambda 1550.774$ ) to vary between 1 and 2 to obtain the best fit<sup>3</sup>. We detected faint broad wings in these lines arising from the BLR, and we fitted these with cubic splines constrained to show a single inflection at zero  $\text{km s}^{-1}$  in the region  $-2000$  to  $+2000 \text{ km s}^{-1}$ . We show in Figure 3 that our method provides an excellent fit to the observed profiles, and allows an accurate deconvolution of the NLR, ILR, and BLR contributions to the emission lines.

From the deconvolution of the emission-line profiles, we determined the line ratios for the narrow and intermediate-width components. Table 2 gives these line ratios relative to He II  $\lambda 1640$ . Based on the deconvolution procedure, the uncertainties in the line ratios are in the range  $10 - 20\%$ . For comparison, we give the line ratios from an FOS spectrum obtained on 1992 July 5, when NGC 5548 was in its previous very low state (Crenshaw, Bogges, & Wu 1993; Kraemer et al. 1998). Although the FOS spectrum is from a larger aperture ( $1''.0$  circular), and therefore includes more NLR flux, and the FOS spectral resolution is not sufficient to separate the narrow and intermediate-width components, the FOS line ratios are

---

<sup>3</sup>Although one might expect a doublet ratio of 2, the optically thin value, observational evidence for a ratio of  $\sim 1$  for the O VI emission line doublet in the NLR of NGC 1068 is given by Kriss et al. (1992). We suspect that the narrow emission line doublet ratios are affected by resonance line scattering within the outflow, and we will explore this in a future paper.

very similar to those from the combined narrow and intermediate components in the STIS data. The STIS intermediate-line ratios relative to He II are slightly higher than those from the narrow component, but are again very similar. In Kraemer et al. (1998), we found that the NLR was reddened by  $E_{B-V} \approx 0.07$ . Assuming this value holds for both components in the STIS data, we give reddening-corrected ratios and He II fluxes in Table 2 based on a standard Galactic reddening curve (Savage & Mathis 1979).

The strong C IV line provides the best opportunity for deconvolving the emission-line components in the other three epochs of observation, and we did this using the same procedures and templates described above. Figure 4 shows the light curves for the C IV emission components and the continuum flux at 1360 Å. It is important to note that the continuum variations are highly undersampled over this time period; the UV continuum in NGC 5548 can vary significantly (factor of  $\sim 2$ ) over time scales of days to weeks (Clavel et al. 1991). Nevertheless, the overall trend from 1998 to 2004 appears to a large-scale decrease in the continuum flux in the UV and in other wavebands, as discussed in §1.

The NLR emission component has stayed constant to within the uncertainties over  $\sim 8$  years, consistent with an origin from an extended region (constrained by the aperture to be  $\sim 70 \times \sim 70$  pc in the plane of the sky and possibly larger in the line of sight). The BLR shows large-amplitude C IV variations that are strongly correlated with those of the UV continuum, consistent with previous results from more intensive UV monitoring (Clavel et al. 1991) that the size of the C IV BLR is on the order of light days. The ILR flux appears to show a slight decline on a time scales of years, consistent with a delayed response to the long-term decline in continuum flux, indicating a size on the order of light years for the ILR.

Due to the close agreement between the ILR line ratios and those from our FOS observations of NGC 5548 in a low state, we can adapt our previous photoionization models of the FOS data to model the ILR emission-line ratios. In Kraemer et al. (1998), we required two components, INNER and OUTER, to match the FOS line ratios. INNER is the appropriate model to use for the ILR, since it contributes essentially all of the N V and C IV emission. We have recalculated INNER using CLOUDY, version 07.02.01, last described by Ferland et al. (1998). We used the same parameters as before ( $U = 10^{-1.5}$ ,  $n_H = 10^7 \text{ cm}^{-3}$ ,  $N_H = 10^{21.5} \text{ cm}^{-2}$ ), the same SED as in Paper II, and roughly solar abundances (see §5). We have verified that the resulting line ratios agree well with our previous model calculations. In Table 3, we show that there is good agreement between the dereddened UV line ratios from the ILR and those from our model. The underprediction of N V is a common problem for photoionization models of the NLR (see Kraemer, Bottorff, & Crenshaw 2007 for a possible solution).

#### 4. Intrinsic Absorption Lines

We list the kinematic components of absorption and their radial velocity centroids in Table 4. In Paper II, component 6 was only detected in Ly $\alpha$ , and it is not considered in the current paper. Before we discuss the detailed measurements of the absorption lines, we point out a couple of interesting aspects of the features in Figure 3. First, the maximum velocity of the absorption roughly coincides with the maximum extent of the blue wings of the ILR profiles, which was also the case for NGC 4151 (Crenshaw & Kraemer 2007). Although this may just be a coincidence, it suggests a possible connection between the absorption and emission regions. Second, the ILR fluxes at the positions of absorption components 2 – 5 in Ly $\alpha$  exceed the residual fluxes in the absorption troughs, indicating that these absorption components at least partially cover the ILR. Component 1, on the other hand, is not required to cover the ILR.

We have adopted two different procedures for measuring the ionic column densities of the absorption lines. The first procedure, based on an approach that has been used extensively in the past, including in Papers I and II, assumes that the absorber partially covers the different background emission components by the same fraction, except for the NLR. For the current data, this procedure leads to serious problems with the physical interpretation of the absorbers, as discussed in the next subsection. The second procedure assumes different covering factors for each of the emission components, and makes a few straightforward assumptions to derive ionic columns that do not result in major problems in the interpretation.

##### 4.1. Partial Covering of All Emission Components except the NLR

There is extensive evidence that the NLR emission in other Seyfert galaxies is not, in general, covered by the intrinsic UV absorbers (Arav, de Kool, & Korista 2002; Kraemer et al. 2002; Gabel et al. 2003; Crenshaw & Kraemer 2007). If we assume that the NLR is uncovered and that all of the other emission components are covered by the same fraction, then we can use the traditional doublet method (Hamann et al. 1997) to determine the line-of-sight covering factors ( $C_f$ ) and ionic column densities of the absorption components. The only modification to our approach in Papers I and II is that we have now isolated the NLR and ILR emission, whereas previously we had assumed a single emission component in the core that is partially covered. The current approach yields essentially identical columns for our previous data, because the NLR only contributes to the region around absorption component 5, and in a relatively minor way (see Figure 3).

Based on the above assumptions, we can determine the covering factors from the C IV and/or N V doublets from

$$C_f = \frac{I_1^2 - 2I_1 + 1}{I_2 - 2I_1 + 1}, \quad (1)$$

where  $I_1$  and  $I_2$  are the residual normalized fluxes in the weaker line (e.g., C IV  $\lambda 1550.8$ ) and stronger line (e.g., C IV  $\lambda 1548.2$ ), respectively.

The optical depth at a particular wavelength is then given by

$$\tau = \ln \left( \frac{C_f}{I_r + C_f - 1} \right) \quad (2)$$

For the current data, we subtracted the NLR emission from the observed spectrum, and normalized the absorption profiles by dividing by the sum of the remaining emission components (continuum, BLR, ILR). We then determined the covering factors in the troughs of the lines from equation 1. We were unable to measure covering factors as a function of radial velocity across the absorption lines, due to blending in the wings of the components and because the spectrum in this very low state is still somewhat noisy despite the long exposure time (see Figures 1 and 3). For components 1 and 5, one member of each of the C IV and N V doublets is affected by blending with another line. For these components, we assumed  $C_f = 1.0$ , as in Paper II. For components 2, 3, and 4, our values are  $C_f = 0.68$  ( $\pm 0.08$ ),  $0.63$  ( $\pm 0.06$ ), and  $0.84$  ( $\pm 0.06$ ), respectively. These values are slightly lower than those derived in Paper II, but agree to within the uncertainties. We converted the normalized absorption to optical depth profiles by using the above covering factors and integrating across the profiles to obtain the ionic column densities (see Crenshaw et al. 2003).

In order to examine the variability of the ionic columns, we combine our current measurements with those from Papers I and II. In Figures 5 – 9, we plot the continuum fluxes, ionic column densities of N V and C IV, and the ratio of these columns as a function of Julian Date for each of the five components (all indicated with a “+” symbol). Based on the sparse data points, the UV continuum flux increased from 1996 to 1998, and declined dramatically thereafter through 2002 and 2004. Component 1 showed a steady increase in the N V and C IV columns from 1998 to 2004 (last 3 points), but no evidence for a change in the N V/C IV ratio. Component 2 showed no evidence of column variations outside of the error bars. Component 3 showed significant N V and C IV variations, but, again, no evidence for a change in the ratio.

Components 4 and 5 in Figures 8 and 9 show an unusual trend. The N V/C IV ratios appear to have decreased significantly from 2002 to 2004, consistent with the decrease in the UV continuum and a drop in the ionizing flux. However, the ionic column densities of



N V and C IV *dropped* as well, except for C IV in component 5. Based on our previous photoionization models of these components in Paper II, we would expect that the N V and C IV columns would *increase* with decreasing flux if the total column, characterized by  $N_H$ , stayed the same. The only way to obtain the observed N V and C IV columns is to have a huge decrease ( $>$  factor of 10) in  $N_H$ . However, these absorbers cover a significant fraction of the ILR, which is on the order of light years in size, and a large drop in  $N_H$  requires a transverse velocity on the order of the speed of light, which is clearly unphysical, especially given the low radial velocities. Thus, we must investigate the possibility that our initial assumptions used to derive the column densities were incorrect.

#### 4.2. Different Covering Factors for Each Component

The different emission components in our STIS aperture have very different size scales, and there is significant evidence that UV absorbers are typically at intermediate distances of tenths to tens of parsecs from the central continuum source (Crenshaw et al. 2005). Thus, a reasonable assumption is that the BLR and continuum source are fully covered, the ILR is partially covered, and the NLR is not covered by the absorbers. However, when we measured the ionic column densities based on this assumption, we obtained values that were only slightly larger than those in the previous section. This simple assumption still results in a huge drop in  $N_H$  from 2002 to 2004 for components 4 and 5, and leaves us with unacceptably large transverse velocities.

If we examine the profiles in Figure 3, we can see that a component of continuous emission that is constant over time, rather than a constant fraction of the emission, might be the key to resolving the above problem. This is a promising avenue of investigation because the relative contribution of such a component to the total emission would be much greater in the N V region, where the ionic column discrepancies are much larger than those in the C IV region, particularly for components 4 and 5 in 2002 and 2004. The constant low-level flux may be due to starlight from a young population (see §6.1) or to emission from an extended scattering region, which we have suggested for NGC 4151 (Kraemer et al. 2001). Because we don't know *a priori* the exact shape of this uncovered emission, we made the simple assumption that it is given by our simple fit to the observed UV continuum points in 2004.

We therefore assumed that the BLR is covered, the ILR is partially covered, and the remaining UV continuum and NLR fluxes shown in Figure 3 are uncovered for absorption components 2 – 5. Our main purpose is to show that a *plausible* background emission model can explain the discrepancies encountered in the previous section. For component 1, we

assumed that the BLR is covered, and the remaining emission is uncovered, because we have no evidence for partial covering of the ILR by component 1. Once again, we subtracted the uncovered components and normalized the profiles by dividing by the remaining emission components. In order to separate out the covering factors of the ILR, we further assumed that the Ly $\alpha$  absorption is completely saturated in components 2 – 5, which is a very safe assumption given the strength of the Ly $\beta$  absorption in previous *FUSE* observations (Brotherton et al. 2002). The residual normalized intensities in the Ly $\alpha$  troughs of components 2 – 5 can be expressed as

$$I_r = R_b(1 - C_f^b) + R_i(1 - C_f^i), \quad (3)$$

where  $C_f^b$  and  $C_f^i$  give the fractional covering of the BLR and ILR, and  $R_b$  and  $R_i$  are the fractional contributions of the BLR and ILR to the occulted emission (Ganguly et al. 1999, Gabel et al. 2003). Because we are assuming that  $C_f^b = 1$ , the covering factor of the ILR is just  $C_f^i = (1 - I_r/R_i)$ . We give the covering factors derived in this manner in Table 4. The major effect of this new procedure on the measurements of the ionic columns is the removal of a substantial amount of background emission before the profiles are normalized.

The “effective” covering factor for each line can be determined from

$$C_f = R_b C_f^b + R_i C_f^i = R_b + R_i C_f^i \quad (4)$$

(Gabel et al. 2003), which we used in equation 2 to determine new values for the ionic column densities. We give the ionic column densities derived from this approach for the 2004 spectra in Table 5. We applied the above technique to the previous GHRS and STIS spectra, and found that the ionic columns did not change appreciably, because the assumed unocculted continuum flux from 2004 does not contribute significantly to the observed emission in the previous observations. We therefore give our previously measured columns from Paper II in Table 5. We did not detect Si IV (or any other lower-ionization line) in the 2004 spectra and we therefore give an upper limit on its column density in the table. Due to serious blending of the Ly $\alpha$  components, we did not attempt to measure lower limits to the H I column densities in the 2004 data; our previously determined limits should be sufficient.

We plot our revised column densities and ratios for the 2004 data in Figures 5 – 9 (indicated with an ‘X’ and offset by +50 days). For components 4 and 5, there is no longer any evidence that the N V/C IV ratio changed over the years of observation, given the uncertainties, and little, if any, evidence that the ionic columns changed. Component 2 still shows no evidence for changes in column density. Components 1 and 3 show a constant N V/C IV ratio to within the errors, and thus no evidence for ionization changes, but both show variable ionic column densities (as we claimed in Paper II), indicating variations in the total hydrogen column density ( $N_H$ ). For component 1, a variable  $N_H$  is not a problem, but rather an indication that the absorber does not cover the ILR and that its column density

in front of the BLR has increased dramatically. Component 3 is broad and irregular, and its structure suggests that it may consist of several subcomponents (see Figure 1). A possible explanation for the variability of component 3 is that it has at least one subcomponent that does not cover the ILR and has a variable  $N_H$  column, due, for example, to bulk motion of the gas across the BLR.

## 5. Photoionization Models of the Absorbers

To explore the physical conditions in the absorbers, we calculated photoionization models with CLOUDY to match the observed ionic column densities from each of the STIS observations. We modeled the absorbers as matter-bounded slabs of atomic gas, irradiated by the central source. We do not have constraints on the relative radial positions of the absorbers, and we therefore did not explore the effect of filtering of the ionizing radiation (e.g. Kraemer et al. 2006). As per convention, the models are parameterized in terms of the dimensionless ionization parameter  $U$ , the ratio of the density in photons with energies  $\geq 13.6$  eV, to the number density of hydrogen atoms at the illuminated face of the slab, and the total hydrogen column density  $N_H$  ( $= N_{HI} + N_{HII}$ ), in units of  $\text{cm}^{-2}$ . As mentioned in §3, the spectral energy distribution (SED) is detailed in Paper II. Because simultaneous X-ray observations only exist for the 2002 dataset, we assumed the same SED for each observation.

As described in Paper II, we initially modeled the absorbers using roughly solar abundances (e.g., Grevesse & Anders 1989), which were by number relative to H: He=0.1, C=  $3.4 \times 10^{-4}$ , N=  $1.2 \times 10^{-4}$ , O =  $6.8 \times 10^{-4}$ , Ne =  $1.1 \times 10^{-4}$ , Mg=  $3.3 \times 10^{-5}$ , Si =  $3.1 \times 10^{-5}$ , S=  $1.5 \times 10^{-5}$ , Fe=  $4.0 \times 10^{-5}$ . Note that new methods for the determination of elemental abundances in the Sun (e.g., Grevesse & Sauval 1998), suggest that solar abundance ratios, in particular that of nitrogen, are somewhat less than those we had assumed. However, there is evidence that these “old solar” values are approximately correct for the NLR in Seyfert galaxies (e.g. Groves, Dopita, & Sutherland 2004).

The N V and C IV column densities and their ratios are sensitive to  $U$  and  $N_H$ , and they can therefore be used to constrain the model parameters. In Paper II, the above solar abundance models predicted larger O VI column densities than those determined from non-simultaneous *FUSE* observations by Brotherton et al. (2002). This led us to generate additional sets of models with higher N/C abundance ratios, which has the effect of reducing  $U$  and  $N_H$ , and, therefore, the O VI column. However, the *FUSE* observations were obtained through a very large ( $30'' \times 30''$ ) aperture, when NGC 5548 was in a low state (similar to the 1992 July observation with the FOS). If there is a significant component of extended UV continuum emission, as we suggest in §4, the *FUSE* O VI and Ly $\beta$  columns in Brotherton

et al. (2002) are severely underestimated, as originally found by Arav, et al. (2003), and we can no longer use them as constraints on our models. Thus, there is no need to include models that assume supersolar N/C.

Our approach in modeling the absorbers was as follows. Updates in the available atomic data prompted us to rerun the models detailed in Paper II with the latest version of Cloudy. This resulted in only slight differences in  $U$  and  $N_H$  compared to our previous models. Our models were deemed successful when the predicted column densities for N V and C IV were within 5% of the measured values, and the lower and upper limits for H I and Si IV, respectively, were met. The one exception is the 1998 STIS observation, for which we were only able to obtain an upper limit for C IV; in this case, we only required that the predicted N V column match the measured values to within the uncertainties. The final model parameters and the predicted ionic column densities are given in Tables 6 and 7, respectively.

In Table 6, the variations in  $U$  and  $N_H$  at different epochs reflect, for the most part, the uncertainties in our measurements. In particular, the components that we suggest are not variable outside of the error bars (components 2, 4, and 5) show values of  $U$  and  $N_H$  that are the same to within a factor of  $\sim 2$  or less. The same goes for  $U$  in components 1 and 3. However, the column densities ( $N_H$ ) in components 1 and 3 change by as much as a factor of 10, in agreement with our claim in the previous section.

Given the overlap in outflow velocities between the UV and X-ray absorbers (Steenbrugge et al. 2005), it seems plausible that there is a footprint of the X-ray absorbers in the UV. According to Table 6, the only possible candidate for a combined UV/X-ray absorber is component 3, which has a much higher  $U$  and  $N_H$  than those of the other components. In Table 8, we compare the predicted X-ray column densities from component 3 to those derived by Steenbrugge et al. (2005), from the contemporaneous *Chandra*/HETG and LETG spectra for their Model B, for which they derived the outflow velocities rather than fixing them to those of the UV absorbers. Although there are several discrepancies, the overall match is reasonable (an additional higher-ionization component would likely eliminate some of these discrepancies). Interestingly, the average outflow velocities derived by Steenbrugge et al. were generally in the range of  $-400$  to  $-800$  km s $^{-1}$ , which encompass those of UV components 2 – 4. Hence, it is plausible that Component 3 produced much of the X-ray absorption detected in the *Chandra* spectra in 2002.

## 6. Discussion

### 6.1. Nature of the Extended UV Emission

The two candidates for the uncovered UV continuum emission in the 2004 spectrum of NGC 5548 are: 1) scattered nuclear radiation by electrons or dust in the inner NLR, and 2) emission from hot stars within the aperture. The first option is not very likely, because the spectrum of the scattered radiation should include both continuum and BLR emission. However, as shown in Figure 3, absorption component 4 absorbs nearly all of the emission at its position, leaving very little room for scattered broad  $L\alpha$  emission. Hence, it is unlikely that the extended emission contains a significant component of broad emission, indicating that it is not likely due to scattered radiation from the nucleus.

Evidence for emission from hot stars in the circumnuclear region of NGC 5548 can be found in the *HST* F330W (U-band) image obtained on 2003 March 17 (Muñoz Marín et al. 2007), which shows UV emission from a star-forming region along an inner spiral arm  $\sim 2''$  NE of the nucleus, as well as UV emission from other stellar clusters further away. The inner  $\sim 1''$  of this image is dominated by the PSF of the AGN, which we modeled with the image of a star observed in the same configuration. We first convolved the image of NGC 5548 with a Gaussian function to match the resolution of the PSF star. We measured the fluxes of NGC 5548 from this convolved image and the PSF star inside concentric circular apertures, increasing the radius in 0.5 pixel steps. Figure 10 shows the resulting radial brightness profiles of NGC 5548 and the PSF star normalized to the continuum peak flux. This figure also shows the subtraction of the PSF profile, scaled by factors of 0.6, 0.75 and 0.8, from the profile of NGC 5548. An inspection of the figure indicates that a scaling factor between 0.75 and 0.8 produces the best residuals, by not significantly oversubtracting the nucleus and effectively eliminating the large PSF humps at  $0.4''$  and  $0.65''$ . Using the PSF subtracted profiles we calculate that the  $3360 \text{ \AA}$  extended flux inside a region of  $0''.2$  is  $1.1 \pm 0.1 \times 10^{-15} \text{ erg s}^{-1} \text{ cm}^{-2} \text{ \AA}^{-1}$ . This value translates to  $2.5 \pm 0.2 \times 10^{-15} \text{ erg s}^{-1} \text{ cm}^{-2} \text{ \AA}^{-1}$  at  $1360 \text{ \AA}$  for  $F_\lambda \propto \lambda^{-1}$ . This is completely consistent with our estimate for the uncovered UV continuum emission in the STIS spectra of  $F_\lambda(1360 \text{ \AA}) = 2.4 (\pm 0.8) \times 10^{-15} \text{ ergs s}^{-1} \text{ cm}^{-2} \text{ \AA}^{-1}$ .

### 6.2. Constraints on the Mass Outflow

Using our photoionization models for the 2002 epoch and the lack of evidence for a response to the UV continuum decrease from 2002 to 2004, which provides an upper limit of 2.0 yr to the recombination time, we constrained the electron densities in the absorbers

following the method described in Paper II, based on the equation in Bottorff, Korista, & Shlosman (2000). Note, we have assumed radiative recombination rates from Shull & van Steenberg (1982) and dielectronic recombination rates from Nussbaumer & Storey (1983). For components 1, 2, 4, and 5, we derive upper limits for the electron density of  $n_e \lesssim 100 \text{ cm}^{-3}$  and  $300 \text{ cm}^{-3}$ , from C IV and N V, respectively. For component 3, we derived  $n_e \lesssim 25 \text{ cm}^{-3}$  and  $50 \text{ cm}^{-3}$ , respectively. While the model parameters for our solar models are different than the “dusty” models we explored in Paper II, the upper limits for  $n_e$  are similar, primarily due to the shorter time scale examined here.

Given  $U$ , an upper limit on  $n_e$  from N V, and a luminosity of ionizing photons corresponding to an historic mean level for NGC 5548 ( $Q = 1.1 \times 10^{54} \text{ s}^{-1}$ , Kraemer et al. 1998), we calculated the radial distances  $r$  of the absorbers from the ionizing continuum source. For all the UV absorbers,  $r \gtrsim 70 \text{ pc}$ . This limit applies to component 3 as well, because its higher  $U$  is offset by its lower  $n_e$ . From  $U$  and  $n_H$  ( $\approx n_e$ ), we calculated a distance of  $\sim 1 \text{ pc}$  for INNER (Kraemer et al. 1998). This is consistent with the weak response of the ILR to continuum variations on time scales of year. The UV absorbers in NGC 5548 are therefore at much greater distances from the central continuum source than the inferred distance of the ILR, similar to the case for NGC 4151, where the non-ILR absorbers span a range of distances from 1 to 2000 pc (Kraemer et al. 2001). In general, we have found that the radial positions and velocities of most UV absorbers in Seyfert 1 galaxies are consistent with a location in the inner NLR, at distances of tens of pcs from the central continuum source (Crenshaw & Kraemer 2005).

The relatively low ionization parameter  $U$  and large column  $N_H$  of the ILR, compared to the UV absorbers, result in very large columns of N V ( $10^{16.6} \text{ cm}^{-2}$ ) and C IV ( $10^{17.6} \text{ cm}^{-2}$ ). Thus, our line of sight (LOS) is such that we do not see the ILR in absorption against the central continuum source and BLR. From the ionizing continuum and  $H\beta$  luminosities of NGC 5548 in 1992, we estimated that the global covering factor of INNER was  $C_g \approx 0.07$  (Kraemer et al. 1998). Although this is significantly smaller than the global covering factor that we derived for NGC 4151 ( $C_g \approx 0.4$ ), it suggests that our chances of observing very large column densities may be dependent on polar angle with respect to the accretion disk axis. In fact, from kinematic studies of the NLR in NGC 4151 based on STIS spatially-resolved spectra (Das et al. 2005), we find that our viewing angle is  $\sim 45^\circ$  with respect to the outflow axis. Although there are no similar long-slit spectra of NGC 5548, we note that its NLR is compact and nearly circular in appearance (Schmitt et al. 2003), suggesting a smaller viewing angle.<sup>4</sup>

---

<sup>4</sup>However, we note that the radio jet is much more extended ( $\sim 18''$ ) than the NLR ( $\sim 2''.7$ ) in this AGN (Schmitt et al. 2003).

Based on the above results, we present a simplified geometric picture of the mass outflow in NGC 5548 in Figure 11. This figure is similar to one that we presented for NGC 4151 in Kraemer et al. (2001, see Figure 6). The major difference is that the viewing angle for NGC 4151 is significantly larger, just outside of the NLR bicone, and therefore intercepts the ILR (component D+E in NGC 4151, Crenshaw & Kraemer 2007). We have identified at least a portion of component 3 with the X-ray absorption, which Detmers et al. (2007) place at a distance of  $\leq 7$  pc from the nucleus based on its variability in response to a large X-ray continuum drop. The ILR, at a distance of  $\sim 1$  pc, based on our photoionization models and its weak variability on a time scale of years, is not in our line of sight. We depict two possible explanations in Figure 11: 1) the ILR is clumpy and our LOS does not intercept a clump, or 2) the ILR is located at large polar angle and our LOS is at a smaller angle, consistent with the discussion in the previous paragraph. Components 2, 4, 5, and some portion of 3 (which we designate as 3' in Figure 11) are at large distances ( $> 70$  pc), and yet at least 4 and 5 do not completely cover the extended UV continuum source. Component 1 is unusual in that it is at a distance  $> 70$  pc but it does not cover the ILR, because it shows large changes in  $N_H$ , indicating bulk motion across the BLR. The N V emission from the BLR arises in a region with a characteristic size of  $\sim 4$  light days (Korista et al. 1995), which may be a lower limit to the full extent of this region. Given the time interval between the last two observations, the transverse velocity of component 1 is therefore  $v_T \geq 1600$  km  $s^{-1}$ , similar to our previously derived value in Paper 1. The same lower limit applies to the subcomponent of 3 that changed its column density and is likely associated with the X-ray absorber.

Based on the above parameters for the absorbers, we can calculate their mass outflow rates from  $\dot{M}_{out} = 8\pi r N_H \mu m_p C_g v_r$ , where  $m_p$  is the proton mass and  $\mu$  is the mean atomic mass per proton, assuming  $C_g = 0.5$ . For components 1, 2, 4, and 5,  $r \geq 70$  pc and their combined mass outflow rate is  $\dot{M}_{out} \geq 0.92 M_\odot \text{ yr}^{-1}$ .<sup>5</sup> By contrast, the accretion rate into the central SMBH is  $\dot{M}_{acc} = 0.03 M_\odot \text{ yr}^{-1}$ , based on an average bolometric luminosity of NGC 5548 ( $L_{bol} = 1.7 \times 10^{44}$  ergs  $s^{-1}$ , Bentz et al. 2007) and a typical accretion disk radiative efficiency of  $\sim 0.1$  in the conversion of mass infall to energy (Peterson 1997). Thus, the outflow rate at  $> 70$  pc is more than 10 times that of the SMBH accretion rate, similar to the case for NGC 4151 (Crenshaw et al. 2007). The most probable explanation is that most of the infalling gas does not make it to the inner accretion disk, but is instead driven outward at these distances. The combined kinetic luminosity ( $L_{KE} = 1/2 \dot{M}_{out} v^2$ ) of the UV absorbers is  $> 5.6 \times 10^{40}$  ergs  $s^{-1}$ , a lower limit that is nevertheless very small compared to the bolometric luminosity. However, we note that the above mass outflow rate and kinetic luminosity do

---

<sup>5</sup>If a large portion of component 3 is at  $r < 7$  pc, then it has an upper limit of  $\dot{M}_{out} < 12.0 M_\odot \text{ yr}^{-1}$ .

not include contributions from the ILR (if it is in outflow) or the X-ray absorber.

To examine the dynamics of the outflow, we calculated the force multiplier  $FM$ , which is the ratio of radiative acceleration (dominated by line driving) to the acceleration from pure Thomson scattering, for the ionized face and last zone of each absorber model. In order for radiative driving to be efficient,  $FM \geq (L_{bol}/L_E)^{-1}$  (Crenshaw et al. 2003 and references therein). NGC 5548 has a black hole mass of  $M = 6.5 \times 10^7 M_\odot$  (Bentz et al. 2007), which yields an average Eddington ratio of  $L_{bol}/L_E = 0.02$ . Thus the  $FM$  must be  $\geq 50$  in order for radiative driving to be important. For components 1, 2, 4, and 5,  $FM \approx 100$  at the ionized face of the cloud and  $FM \approx 40$  at the back side, so it is plausible that these components are radiatively accelerated. For component 3, which we have linked to the X-ray absorber,  $FM = 20$  and 5 at the ionized and back sides of the absorber, respectively. Thus, as was the case for component D+E (which was also the principal X-ray absorber) in NGC 4151, component 3 in NGC 5548 is not accelerated by radiation driving alone.

To investigate the possibility that component 3 is a thermal wind (Krolik & Kriss 1995, 2001), we calculate the radial distance at which the gas can escape:  $r_{esc} \geq GMm_H/T_gk$  (Crenshaw et al. 2003, and references therein), where  $T_g$  is the gas temperature and  $k$  is the Boltzmann constant. Our photoionization models give  $T_g = 1 \times 10^5$  K, which yields  $r_{esc} \geq 340$  pc. Thus, we cannot rule out a thermal wind for the portion of component 3 at  $d > 70$  pc. However, the X-ray absorber cannot be a thermal wind, and we suggest that magnetocentrifugal acceleration, such as that present in an accretion-disk wind (Bottorff et al. 2000; Everett 2005), may play an important role.

## 7. Conclusions

We have detected a distinct component of emission in a low-state *HST*/STIS spectrum of NGC 5548 that has an intermediate line width with respect to the BLR and NLR in this Seyfert 1 galaxy. The intermediate-line region (ILR) in NGC 5548 is similar to the one that we discovered in NGC 4151 (Crenshaw & Kraemer 2007), although it has a somewhat larger distance from the central continuum source ( $\sim 1$  pc vs.  $\sim 0.1$  pc), smaller velocities (FWHM =  $680 \text{ km s}^{-1}$  vs.  $1170 \text{ km s}^{-1}$ ), and a smaller global covering factor (0.07 vs. 0.4). The source(s) of these differences (e.g., luminosity, evolutionary effects) are not yet known, and detection of this component in other AGN would be useful for exploring the ILR's range in properties.

The major difference in the UV spectra of these two Seyfert 1 galaxies is that we see the ILR in absorption in the form of broad (FWHM  $\approx 500 \text{ km s}^{-1}$ ), highly-saturated absorption



lines in NGC 4151, whereas we do not see the ILR in absorption in NGC 5548. However, given the large UV columns of the ILR in NGC 5548, its spectrum would resemble that of NGC 4151 over a narrow range of viewing angles. Although we have no indication that the ILR in NGC 5548 is in outflow, its resemblance to the ILR in NGC 4151 suggests that this may be the case. Given our relatively large viewing angle of NGC 4151 and the absence of highly-saturated UV lines in most other Seyfert 1 galaxies (Crenshaw et al. 1999), we suggest that ILR gas may be located at a relatively large polar angle (for Seyfert 1 galaxies) of  $\sim 45^\circ$  with respect to the NLR bicone (and likely the accretion disk) axis. At even larger angles, our LOS would presumably be blocked by the putative torus, which suggests, in general, that the column density of absorbing material increases with polar angle. This suggestion is supported by our imaging studies of the NLRs in NGC 4151 (Kraemer et al. 2008) and Mrk 3 (Kraemer et al., in preparation). More determinations of the inclinations of AGN (e.g., from the kinematics of their NLRs) would be extremely helpful in further testing of this hypothesis.

Support for program 9511 was provided by NASA through a grant from the Space Telescope Science Institute, which is operated by the Association of Universities for Research in Astronomy, Inc., under NASA contract NAS 5-26555. Some of the data presented in this paper were obtained from the Multimission Archive at the Space Telescope Science Institute (MAST). SRON is supported financially by NWO, the Netherlands Organization for Scientific Research.

## REFERENCES

- Arav, N., Korista, K.T., & de Kool, M. 2002, *ApJ*, 566, 699
- Arav, N., et al. 2003, *ApJ*, 590, 174
- Bentz, M.C., et al. 2007, *ApJ*, 662, 205
- Bottorff, M.C., Korista, K.T., & Sholsman, I. 2000, *ApJ*, 537, 2000
- Brotherton, M.C., Green, R.F., Kriss, G.A., Oegerle, W., Kaiser, M.E., Zheng, W., & Hutchings, J.B. 2002, *ApJ*, 565, 800
- Clavel, J., et al. 1991, *ApJ*, 366, 64
- Crenshaw, D.M., Boggess, A., & Wu, C.-C. 1993, *ApJ*, 416, L67
- Crenshaw, D.M., & Kraemer, S.B. 1999, *ApJ*, 521, 572 (Paper I)
- Crenshaw, D.M., & Kraemer, S.B. 2005, *ApJ*, 625, 680
- Crenshaw, D.M., & Kraemer, S.B. 2007, *ApJ*, 659, 250
- Crenshaw, D.M., Kraemer, S.B., Boggess, A., Maran, S.P., Mushotzky, R.F., & Wu, C.-C. 1999, *ApJ*, 516, 750.
- Crenshaw, D.M., Kraemer, S.B., & Gabel, J.R. 2001, *ApJ*, 557, 30
- Crenshaw, D.M., Kraemer, S.B., & Gabel, J.R. 2004, in *AGN Physics with the Sloan Digital Sky Survey*, ed. G.T. Richards & P.B. Hall (San Francisco: Astronomical Society of the Pacific), ASP Conference Series, 311, 235
- Crenshaw, D.M., Kraemer, S.B., & George, I.M. 2003, *ARA&A*, 41, 117
- Crenshaw, D.M., et al. 2003, *ApJ*, 594, 116 (Paper II)
- Das, V., et al. 2005, *AJ*, 130, 945.
- Detmers, R.G., Kaastra, J.S., Constantini, E., McHardy, I.M., & Verbunt, F. 2008, *A&A*, 488, 67
- Dunn, J.P., Crenshaw, D.M., Kraemer, S.B., & Trippe, M.L. 2008, *AJ*, 136, 1201
- Everett, J.E. 2005, *ApJ*, 631, 689.
- Ferland, G.J, et al. 1998, *PASP*, 110, 761
- Ganguly, R., Eracleous, M., Charlton, J.C., & Churchill, C.W. 1999, *AJ*, 117, 2594
- Gabel, J.R., et al. 2003, *ApJ*, 583, 178
- Gabel, J.R., et al. 2005, *ApJ*, 631, 741
- Grevesse, N., & Anders, E. 1989, in *AIP Conf. Proc. 183, Cosmic Abundances of Matter*, ed. C.J. Waddington (New York:AIP), 1

- Grevesse, N., & Sauval, A.J. 1998, *Space Sci. Rev.*, 85, 161
- Groves, B.A., Dopita, M.A., & Sutherland, R.S. 2004, *ApJS*, 153, 9
- Hamann, F., Barlow, T.A., Junkkarinen, V., & Burbidge, E.M. 1997, *ApJ*, 478, 78
- Korista, K.T., et al. 1995, *ApJS*, 97, 285
- Kraemer, S.B., Bottorff, M.C., & Crenshaw, D.M. 2007, *ApJ*, 668, 730
- Kraemer, S.B., Crenshaw, D.M., Filippenko, A.V., & Peterson, B.M. 1998, *ApJ*, 499, 719
- Kraemer, S.B., Crenshaw, D.M., George, I.M., Netzer, H., Turner, T.J., & Gabel, J.R. 2002, *ApJ*, 577, 98
- Kraemer, S.B., Schmitt, H.R., & Crenshaw, D.M. 2008 *ApJ*, 679, 1128
- Kraemer, S.B., et al. 2001, *ApJ*, 551, 671.
- Kraemer, S.B. et al. 2006, *ApJS*, 167, 161
- Kriss, G.A., et al. 1992, *ApJ*, 392, 485
- Krolik, J.H. & Kriss, G.A. 1995, *ApJ*, 447, 512
- Krolik, J.H. & Kriss, G.A. 2001, *ApJ*, 561, 684
- Mathur, S., Elvis, M., & Wilkes, B.J. 1999, *ApJ*, 519, 605
- Muñoz Marín, V.M., et al. 2007, *AJ*, 134, 648
- Nussbaumer, H., & Storey, P.J. 1983, *A&A*, 126, 75
- Peterson, B.M. 1997, *An Introduction to Active Galactic Nuclei* (Cambridge, UK: Cambridge University Press).
- Savage, B.D., & Mathis, J.S. 1979, *ARAA*, 17, 73
- Schmitt, H.R., Donley, J.L., Antonucci, R.R.J., Hutchings, J.B., & Kinney, A.L. 2003, *ApJS*, 148, 327
- Shull, J.M., & van Steenberg, M. 1982, *ApJS*, 48, 95
- Steenbrugge, K. C., et al. 2005, *A&A*, 434, 569

Fig. 1.— Spectra of the C IV region in NGC 5548 at four epochs – 1996 (GHRS), 1998 (STIS), 2002 (STIS) and 2004 (STIS). The UV absorption components are numbered for both members of the doublet: C IV  $\lambda$  1548.2 and C IV  $\lambda$  1550.8. Dotted lines give the zero flux level for each spectrum.

Fig. 2.— Spectrum of the He II  $\lambda$ 1640 region from the 2004 STIS echelle observation of NGC 5548. Components of the emission-line plus continuum fits are: continuum + BLR (lower dotted-dashed green), continuum + BLR+ NLR (upper dotted-dashed green), continuum + BLR + ILR (dashed red) and continuum + BLR + ILR + NLR (upper dashed blue). The absorption feature in the red wing of the He II emission is due to Galactic Al II  $\lambda$ 1670.8, which was excluded from the fits.

Fig. 3.— Intrinsic absorption components and emission-line profile fits for portions of the 2004 STIS echelle spectra of NGC 5548, showing the intrinsic absorption lines in different ions. Fluxes are plotted as a function of the radial velocity (of the strongest member, for the doublets), relative to an emission-line redshift of  $z = 0.01676$ . The kinematic components are identified for the strong members of the doublets, and vertical dotted lines are plotted at their approximate positions. Components of the emission-line plus continuum fits are: continuum + NLR (dotted-dashed green), continuum + BLR (upper dotted-dashed red), continuum + BLR + ILR (dashed red) and continuum + BLR + ILR + NLR (upper dashed blue).

Fig. 4.— Light curves of the continuum flux at 1360 Å (bottom panel, in units of  $10^{-14}$  ergs  $s^{-1}$   $cm^{-2}$  Å $^{-1}$ ) and the C IV emission components (top three panels, in units of  $10^{-13}$  ergs  $s^{-1}$   $cm^{-2}$ ).

Fig. 5.— Continuum fluxes (in units of  $10^{-14}$  ergs  $s^{-1}$   $cm^{-2}$  Å $^{-1}$ ), N V and C IV column densities, and N V/C IV column density ratios as a function of Julian Date for absorption component 1. The N V/C IV ratio is not given for the first two dates, because the observations of these two lines were not simultaneous. The original measurements of the 2004 data are represented by a “+”, and the revised measurements based on an uncovered UV continuum source are given by a “X”, offset by +50 days.

Fig. 6.— Same as Fig. 5 for component 2.

Fig. 7.— Same as Fig. 5 for component 3.

Fig. 8.— Same as Fig. 5 for component 4.

Fig. 9.— Same as Fig. 5 for component 5.

Fig. 10.— U-band light profile of NGC 5548 (solid line), a psf star normalized to the peak flux of NGC 5548 (short dash), and three levels of psf subtraction from the galaxy profile. The dotted, long-dashed and dot-dashed lines correspond to the subtraction of a psf normalized to 60, 75 and 80% of the nuclear flux, respectively.

Fig. 11.— Schematic diagram of the emission and absorption sources in the nucleus of NGC 5548 (not to scale). Our exact line of sight is unknown, but it is within the ionization bicone that defines the NLR and not close to the edge of the bicone, as it is for NGC 4151.

Table 1. *HST* High-Resolution Spectra of NGC 5548

Instrument	Grating	Coverage (Å)	Resolution ( $\lambda/\Delta\lambda$ )	Exposure (sec)	Date (UT)
GHRS	G160M	1232 – 1269 <sup>a</sup>	20,000	4607	1996 February 17
GHRS	G160M	1554 – 1590 <sup>b</sup>	20,000	13,600	1996 August 24
STIS	E140M	1150 – 1730	46,000	4750	1998 March 11
STIS	E140M	1150 – 1730	46,000	7639	2002 January 23
STIS	E140M	1150 – 1730	46,000	7639	2002 January 22
New Observations					
STIS	E140M	1150 – 1730	46,000	13,039	2004 February 10
STIS	E140M	1150 – 1730	46,000	13,039	2004 February 11
STIS	E140M	1150 – 1730	46,000	13,039	2004 February 12
STIS	E140M	1150 – 1730	46,000	13,039	2004 February 13

<sup>a</sup>Covers the Ly $\alpha$  and N V regions.

<sup>b</sup>Covers the C IV regions.

Table 2. Emission-Line Ratios (Relative to He II  $\lambda 1640$ )<sup>a</sup>

Component	Ly $\alpha$	N V	C IV
STIS (narrow)	12	1.4	8
STIS (intermediate)	17	1.6	14
STIS (combined)	15	1.5	12
FOS (combined)	12	1.5	9
Reddening Corrected <sup>a</sup>			
STIS (narrow) <sup>b</sup>	14	1.6	8
STIS (intermediate) <sup>c</sup>	20	1.8	14
STIS (combined)	17	1.7	12
FOS (combined)	14	1.7	9

<sup>a</sup>For  $E_{B-V} = 0.07$ .

<sup>b</sup>He II flux =  $2.24 \times 10^{-14}$  ergs s<sup>-1</sup> cm<sup>-2</sup>.

<sup>c</sup>He II flux =  $6.36 \times 10^{-14}$  ergs s<sup>-1</sup> cm<sup>-2</sup>.

Table 3. ILR Emission-Line Ratios<sup>a</sup>

Component	Ly $\alpha$	N V	C IV
Dereddened	20	1.8	14
Model <sup>b</sup>	15	0.9	13

<sup>a</sup>Relative to He II  $\lambda 1640$ .

<sup>b</sup> $U = 10^{-1.5}, n_H = 10^7$  cm<sup>-3</sup>,  
 $N_H = 10^{21.5}$  cm<sup>-2</sup>.

Table 4. Absorption Components in NGC 5548

Comp.	Velocity <sup>a</sup> (km s <sup>-1</sup> )	FWHM (km s <sup>-1</sup> )	$C_f^i$ <sup>b</sup>
1	-1040	220	—
2	-670	40	0.71 ( $\pm 0.04$ )
3	-530	160	0.76 ( $\pm 0.03$ )
4	-340	150	0.96 ( $\pm 0.01$ )
5	-170	60	0.75 ( $\pm 0.04$ )

<sup>a</sup>Velocity centroid for a systemic redshift of  $z = 0.01676$ .

<sup>b</sup>Covering fraction of the ILR, based on the uncovered continuum case.



Table 5. Measured Ionic Column Densities ( $10^{14} \text{ cm}^{-2}$ )

Comp.	Ion	GHRSA	STIS 1998	STIS 2002	STIS 2004 <sup>b</sup>
1	H I	—	>1.34	>2.31	—
	N V	1.98 (0.29)	0.44 (0.18)	2.76 (0.10)	8.13 (2.12)
	C IV	0.11 (0.04)	<0.17	1.12 (0.12)	2.54 (0.56)
	Si IV	—	<0.10	<0.06	<0.22
2	H I	>0.76	>0.61	>1.18	—
	N V	0.90 (0.11)	1.11 (0.16)	1.45 (0.13)	1.52 (0.31)
	C IV	0.39 (0.04)	0.51 (0.07)	0.56 (0.03)	0.68 (0.15)
	Si IV	—	<0.10	<0.06	<0.22
3	H I	>1.79	>2.01	>1.65	—
	N V	7.40 (0.51)	3.04 (0.16)	8.64 (0.56)	6.26 (1.37)
	C IV	0.79 (0.23)	0.45 (0.11)	0.94 (0.26)	1.16 (0.19)
	Si IV	—	<0.10	<0.06	<0.22
4	H I	>3.30	>2.97	>3.64	—
	N V	7.41 (0.87)	10.23 (0.79)	7.26 (0.78)	5.48 (1.47)
	C IV	3.43 (0.35)	3.44 (0.47)	2.70 (0.23)	2.25 (0.53)
	Si IV	—	<0.10	<0.06	<0.22
5	H I	>0.77	>0.66	>0.92	—
	N V	1.05 (0.23)	1.18 (0.24)	1.45 (0.10)	1.55 (0.29)
	C IV	0.41 (0.18)	0.31 (0.13)	0.58 (0.05)	0.77 (0.14)
	Si IV	—	<0.10	<0.06	<0.22

<sup>a</sup>GHRSA C IV is not simultaneous with GHRSA N V and H I.

<sup>b</sup>Based on the uncovered continuum case (see text)

Table 6. Model Parameters

Observation	Component	$\log U$	$\log N_H$
STIS 1998			
	1	−0.50	19.23
	2	−0.84	19.03
	3	−0.12	21.15
	4	−0.60	20.35
	5	−0.48	19.66
STIS2002			
	1	−0.74	19.55
	2	−0.71	19.34
	3	0.10	22.2
	4	−0.68	20.06
	5	−0.72	19.30
STIS2004			
	1	−0.55	20.35
	2	−0.80	19.2
	3	−0.24	21.02
	4	−0.74	19.85
	5	−0.90	19.07

Table 7. Predicted Column Densities( $10^{14} \text{ cm}^{-2}$ )<sup>a</sup>

Comp.	Ion	STIS 1998	STIS 2002	STIS 2004
1	H I	1.52	6.41	22.0
	N V	0.50	2.73	8.11
	C IV	0.14	1.11	2.48
2	H I	2.58	3.60	3.43
	N V	1.14	1.50	1.50
	C IV	0.53	0.58	0.66
3	H I	23.9	88.9	31.0
	N V	3.01	8.51	6.21
	C IV	0.44	0.98	1.12
4	H I	25.9	17.2	12.8
	N V	10.21	7.19	5.53
	C IV	3.39	2.69	2.24
5	H I	3.50	3.38	3.43
	N V	1.13	1.42	1.53
	C IV	0.31	0.56	0.76

<sup>a</sup>Si IV column densities for all models were  $< 10^{12} \text{ cm}^{-2}$ .

Table 8. Predicted<sup>a</sup> and Measured<sup>b</sup> X-ray Column Densities for 2002 spectra

ion	Predicted $\log N_i$	Measured $\log N_i$
C V	16.9	17.2
C VI	18.1	17.6
N VI	17.2	17.2
N VII	18.0	17.5
O V	15.7	16.8
O VI	16.8	16.6
O VII	18.5	18.2
O VIII	18.7	18.5
Ne IX	18.0	17.2
Ne X	17.6	17.9
Mg XI	17.3	17.0
Mg XII	16.5	17.3
Si VIII	16.7	16.2
Si X	17.2	16.0
Si XI	16.8	17.0
Si XIII	16.4	17.0
Si XIV	15.2	17.0
S XI	16.9	16.0
S XII	16.7	16.2
Fe XVII	15.1	16.3

<sup>a</sup>Predicted column densities for component 3 in the STIS 2002 spectra, assuming solar abundances.

<sup>b</sup>Measured columns for Model B of Steenbrugge et al. (2005).

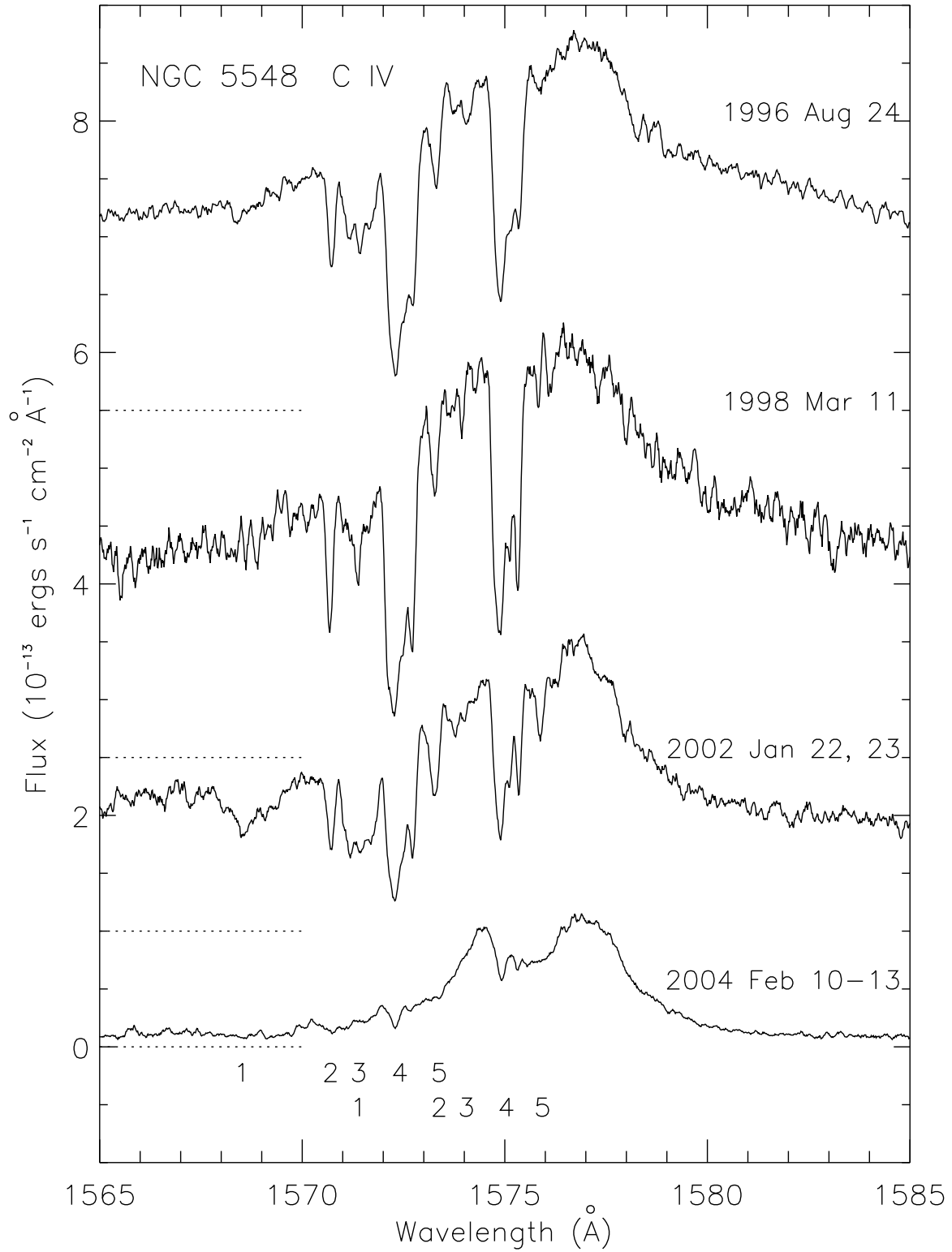


Fig. 1.

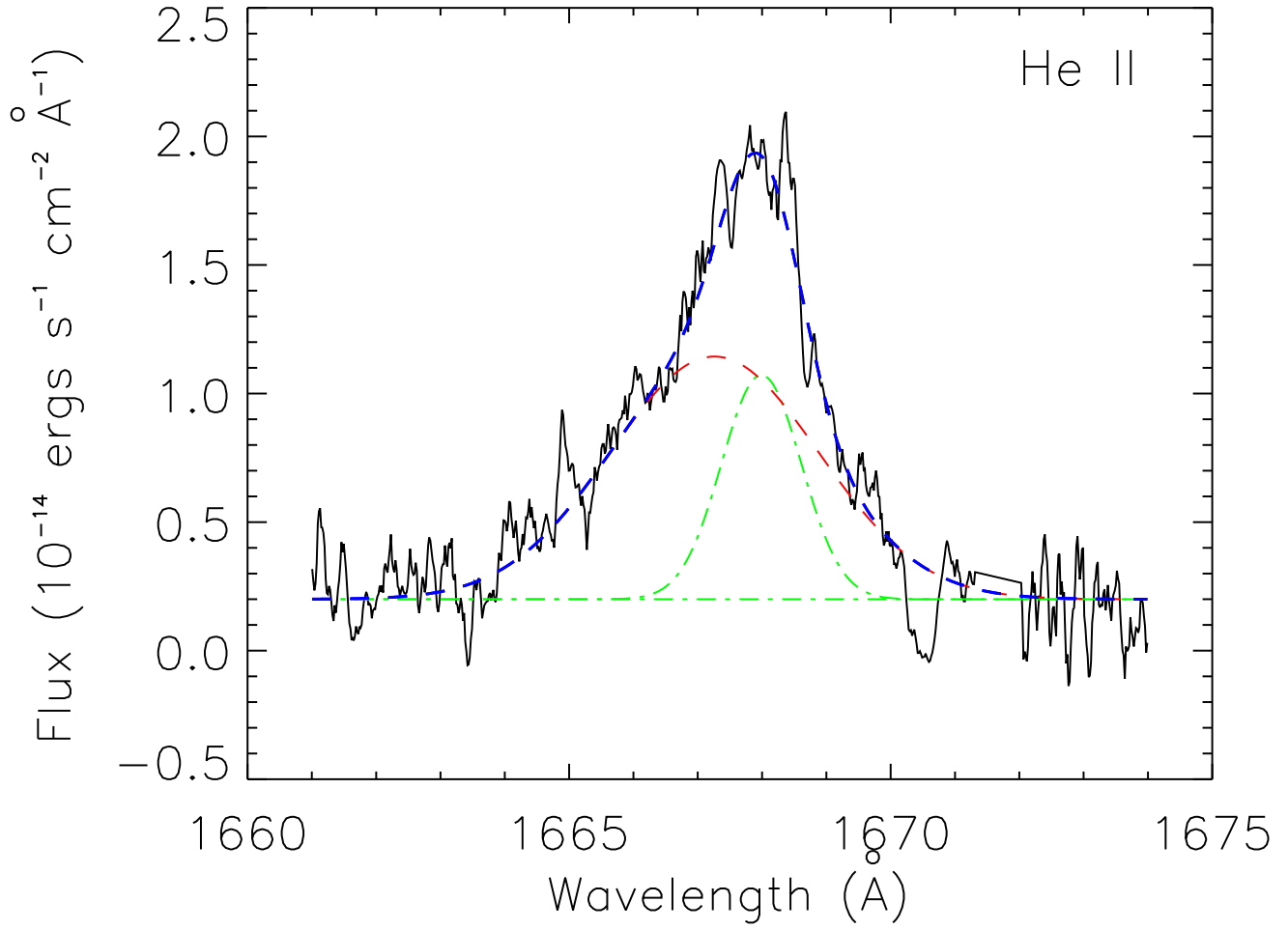


Fig. 2.

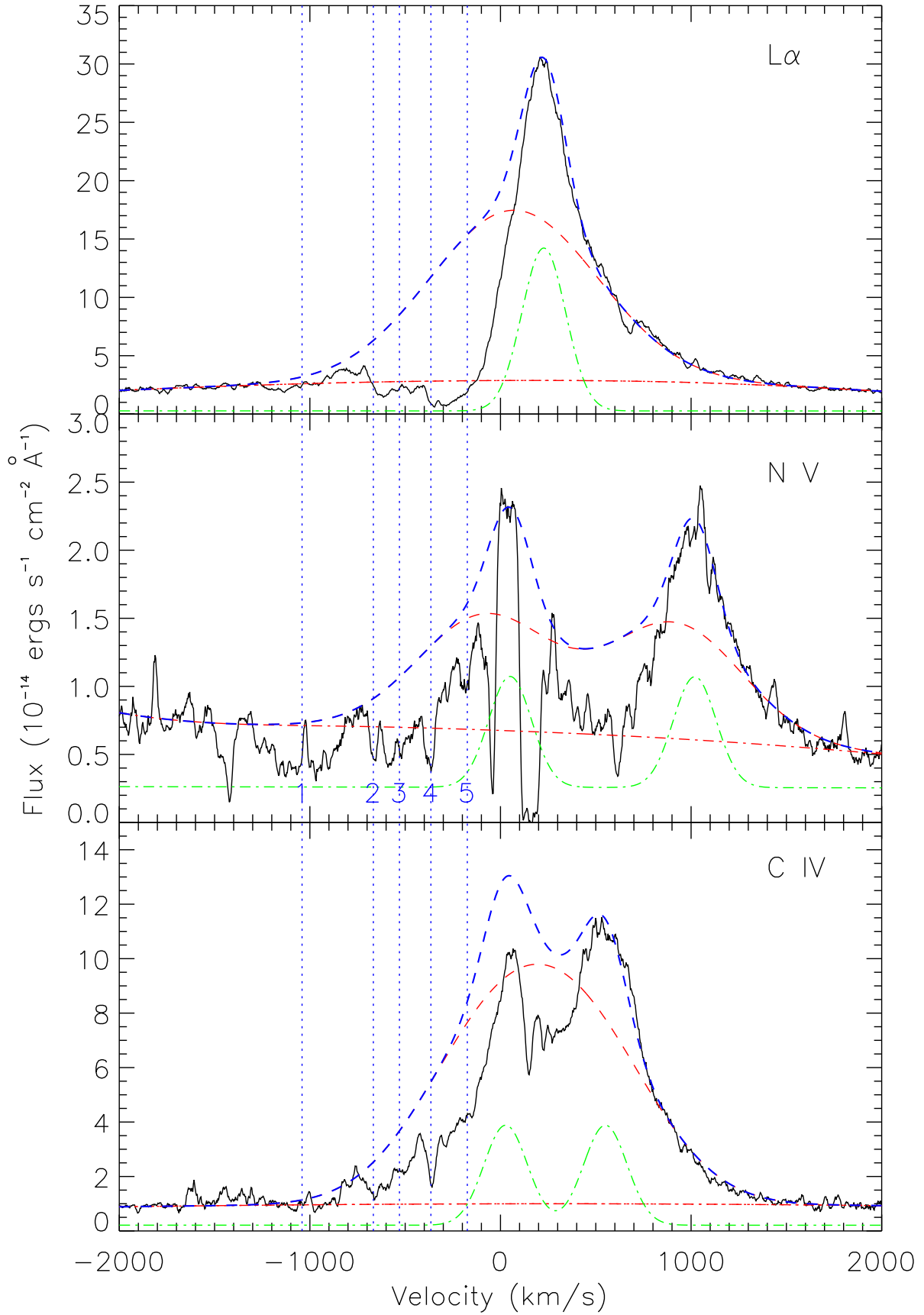


Fig. 3.

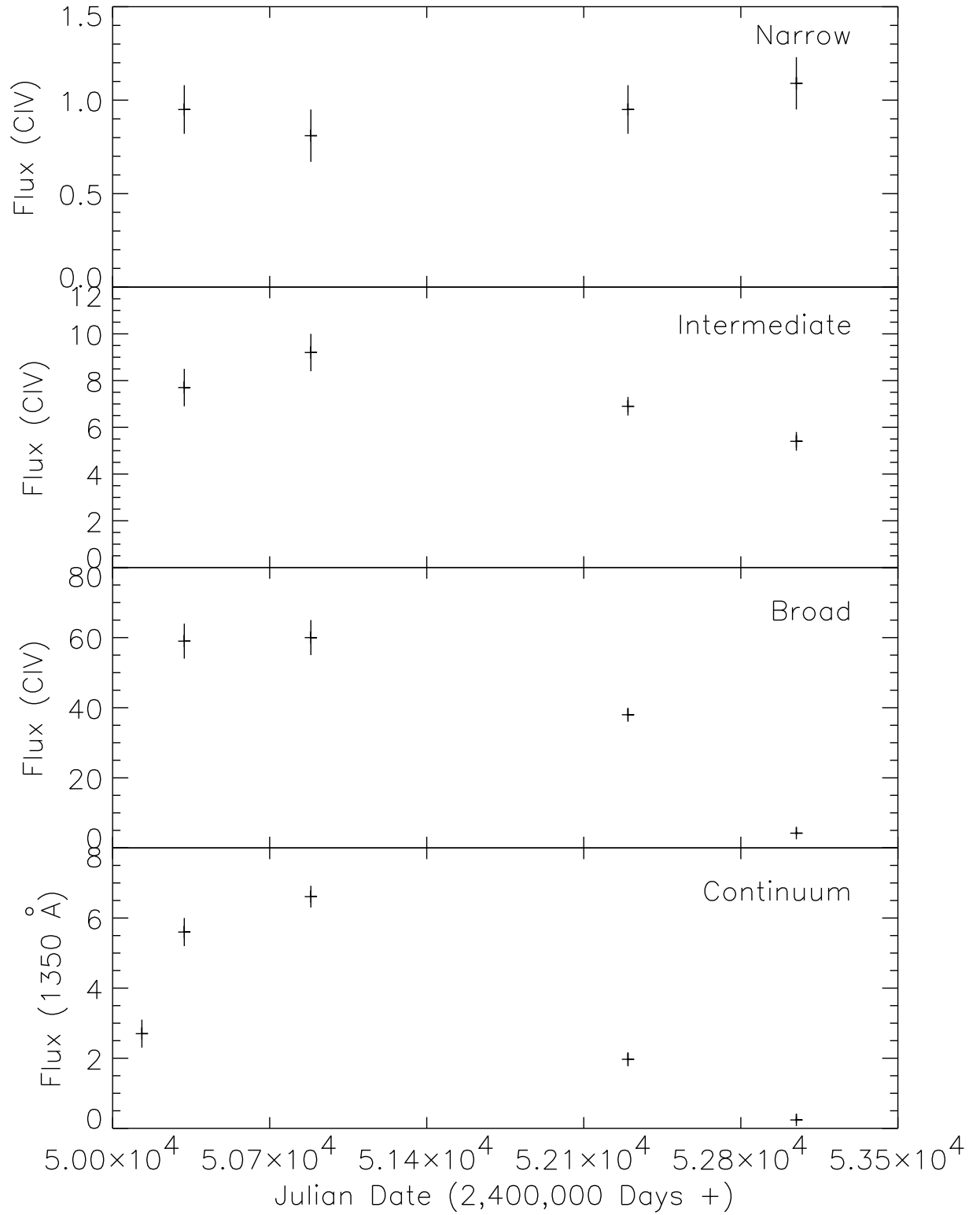


Fig. 4.



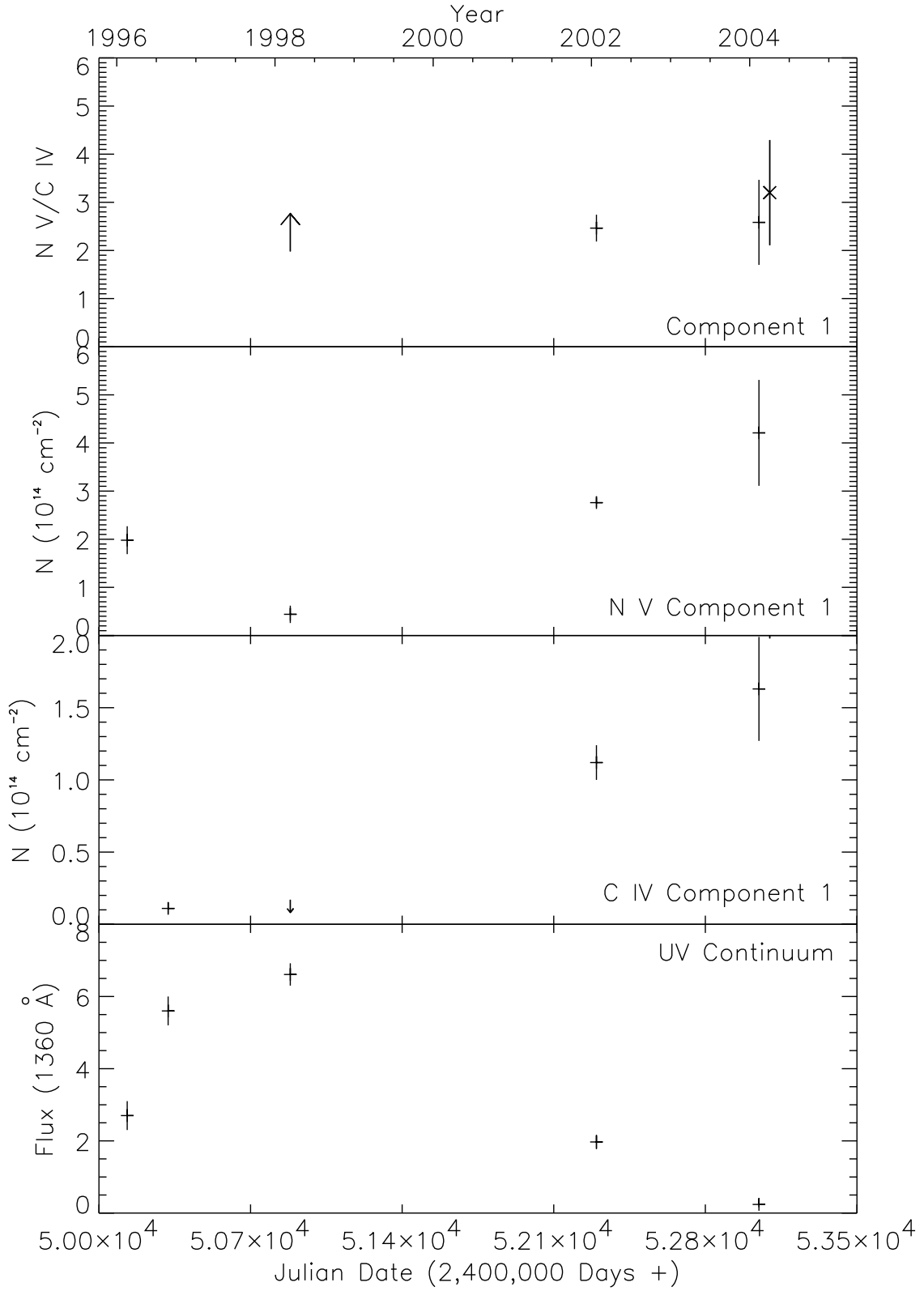


Fig. 5.

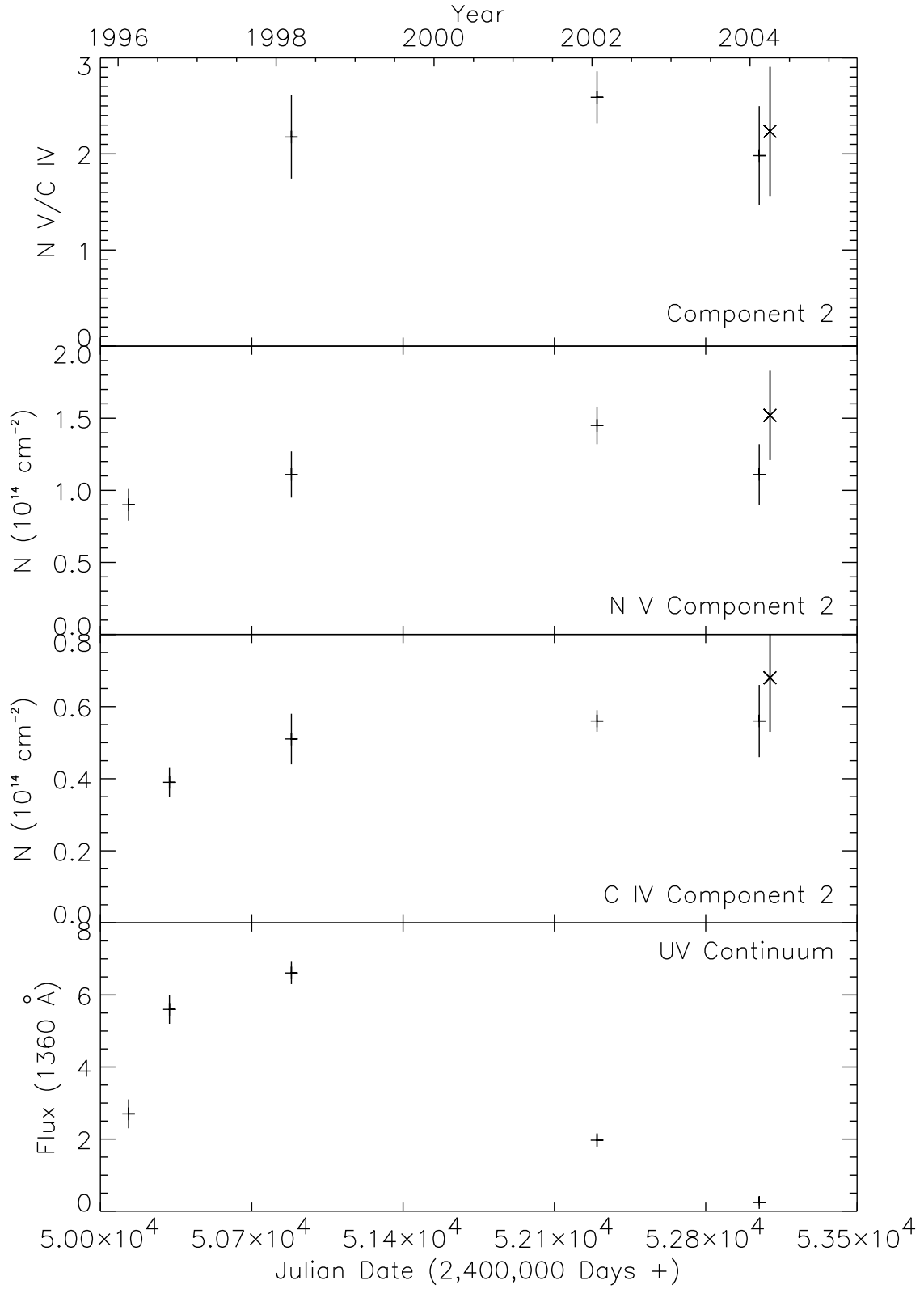


Fig. 6.

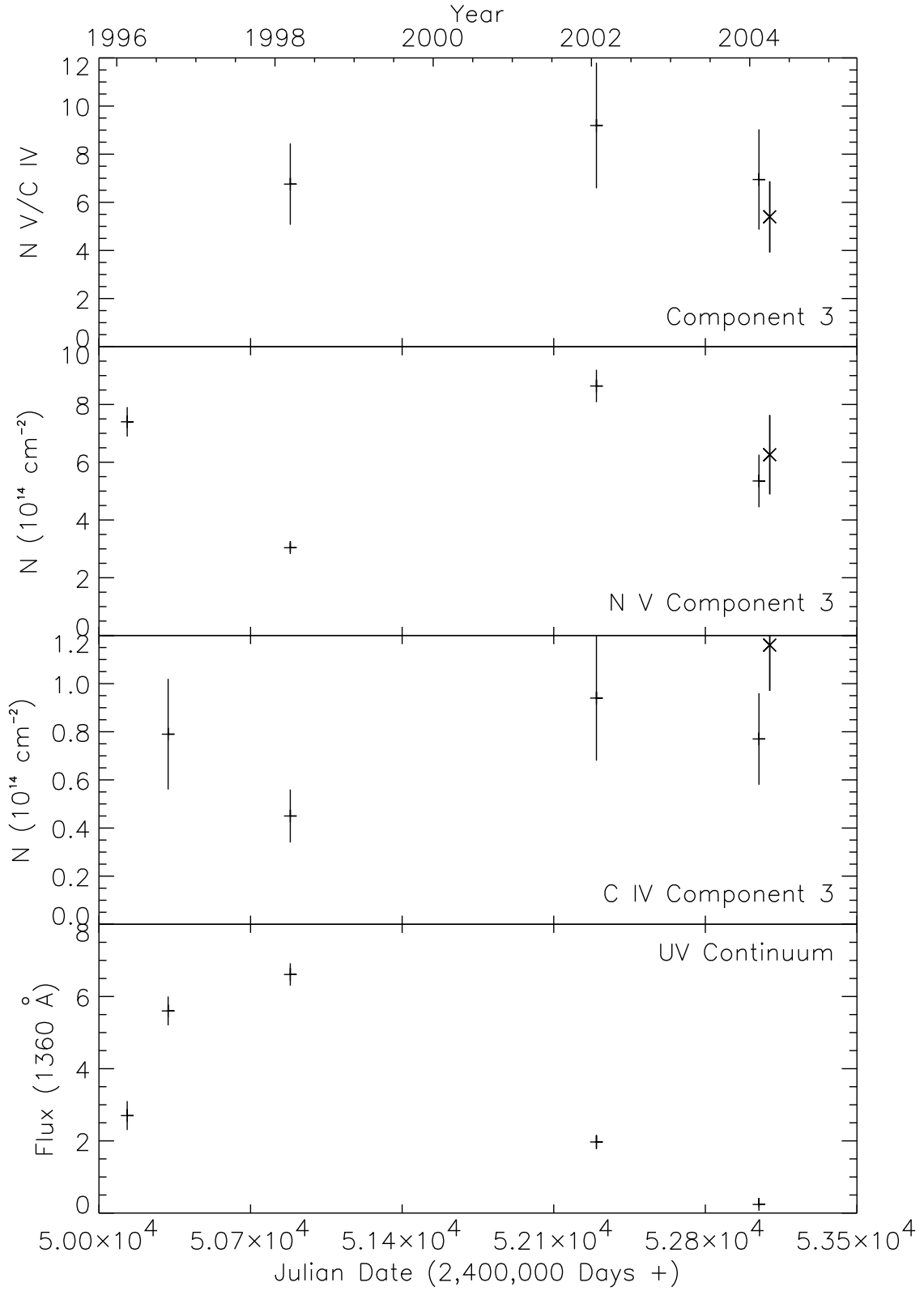


Fig. 7.

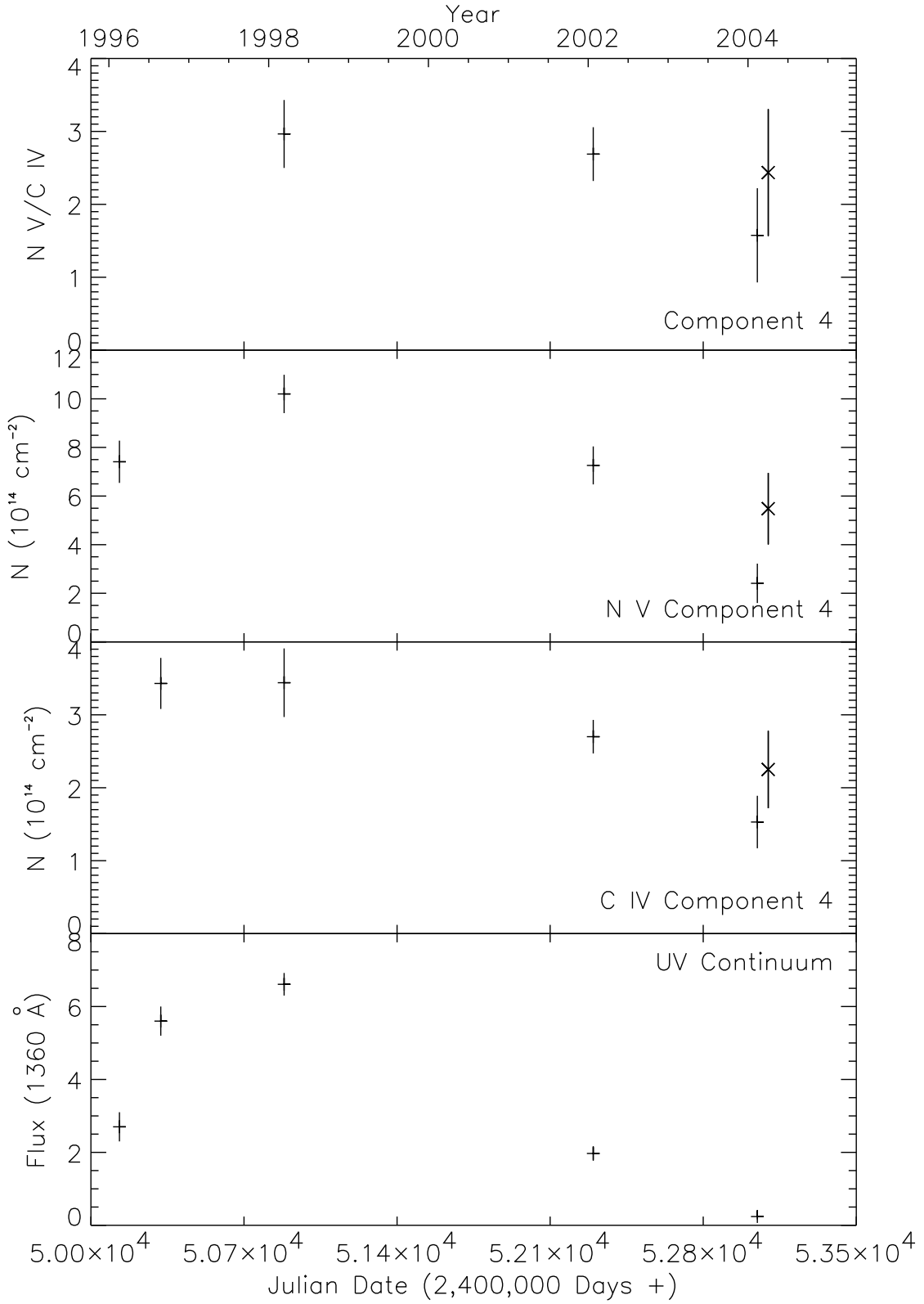


Fig. 8.

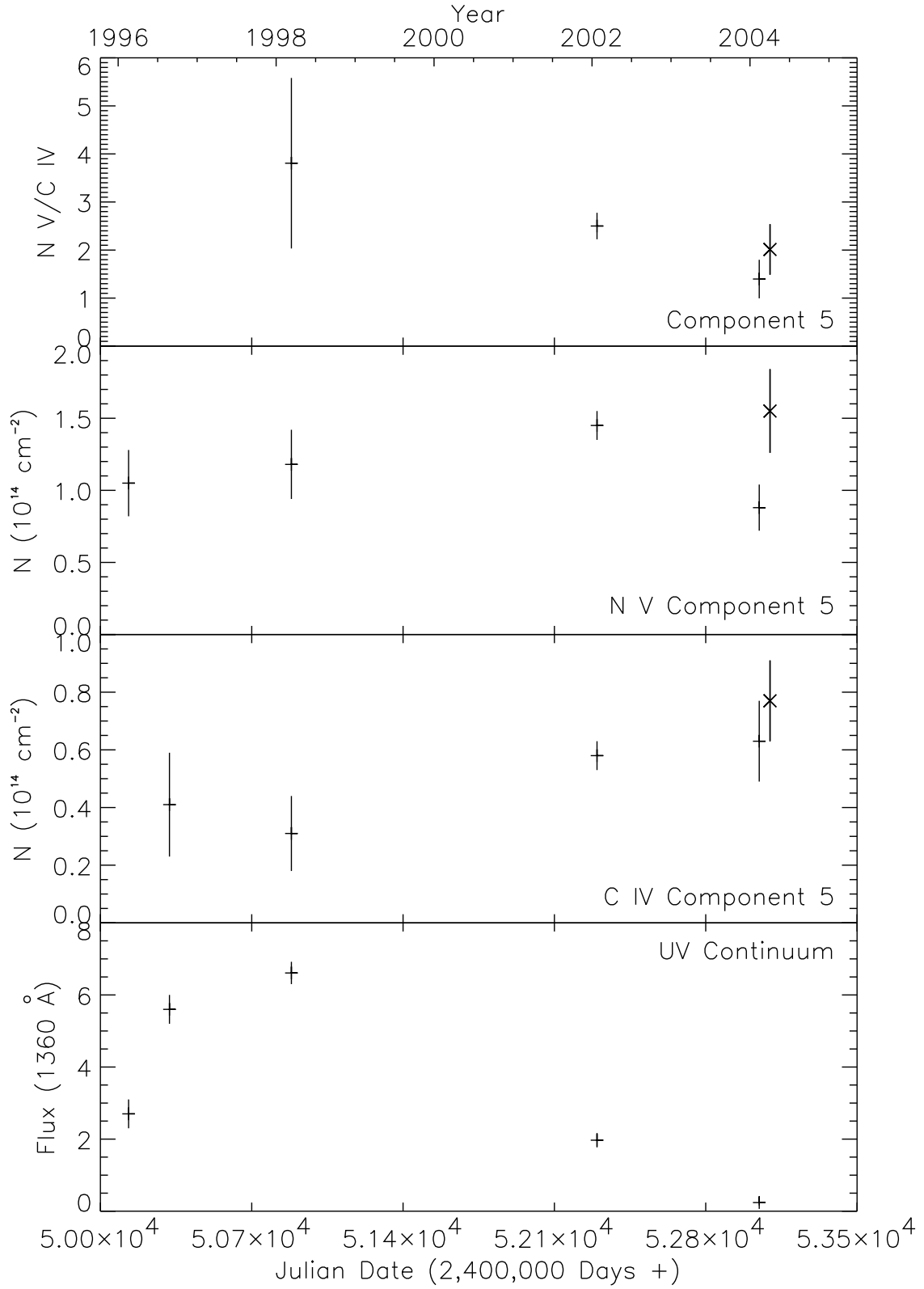


Fig. 9.

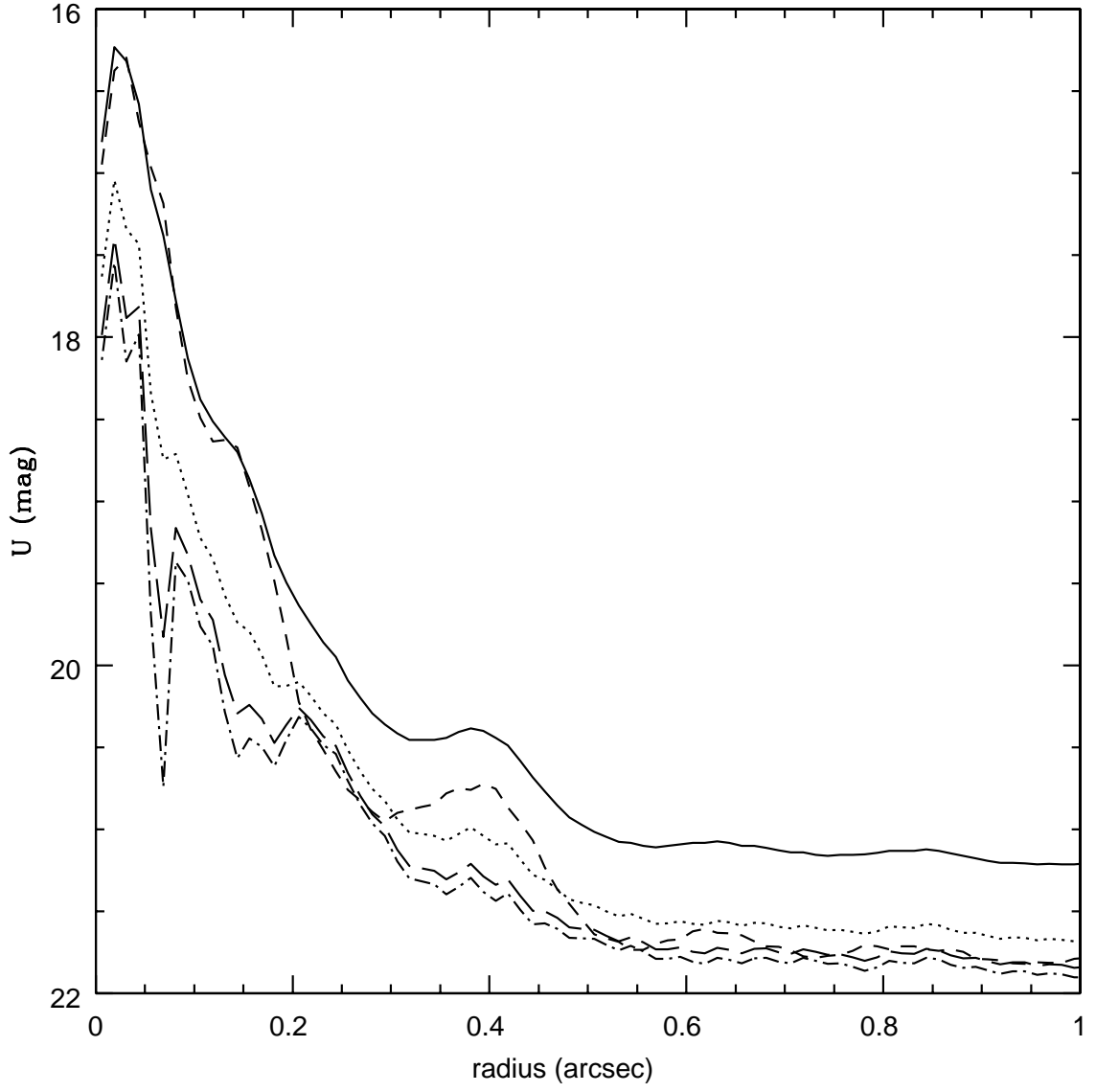


Fig. 10.

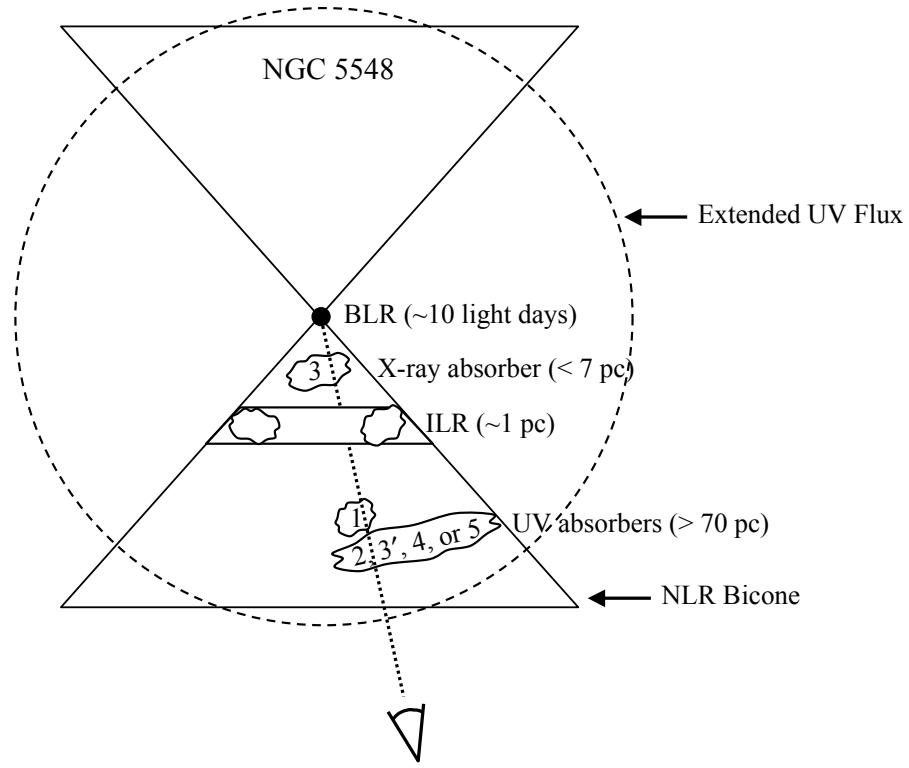


Fig. 11.